Final report of work on NASA grant NASW-4933

"Plasma Properties and Magnetic Field Structure of the Solar Corona, Based on Coordinated Max '91 Observations from SERTS, the VLA, and Magnetographs"

covering the period 12 July 1994 — 11 July 1996

PRINCIPAL INVESTIGATOR:

Dr. Jeffrey W. Brosius
Hughes STX Corporation
4400 Forbes Boulevard
Lanham, MD 20706-4392
Tel.: (301) 286-6200

1 Introduction

The purposes of this investigation were to determine the plasma properties and magnetic field structure of the solar corona using coordinated observations obtained with NASA/GSFC's Solar EUV Rocket Telescope and Spectrograph (SERTS), the Very Large Array (VLA), and magnetographs. The observations were obtained under the auspices of NASA's Max '91 program. I used the SERTS spectra and spectroheliograms to determine coronal plasma properties such as temperature, density, and emission measure. These properties were subsequently used in an IDL computer code which I developed to derive the coronal magnetic field as a function of temperature (B(T)) in each pixel of the two dimensional images. Both thermal bremsstrahlung and thermal gyroemission were incorporated in the calculations. In each pixel the solution for B(T) was the one which minimized the differences between the observed and the calculated 20 and 6 cm microwave intensities. An absolute height scale was difficult to determine, owing to the highly uncertain volume filling factors. Nevertheless, the three-dimensional structure of the coronal magnetic field (x,y,T instead of x,y,z) was determined in such a way as to be consistent with all of the EUV spectra and spectroheliograms, as well as with the intensity and polarization maps at two different microwave observing frequencies. For completeness, I compared the coronal magnetograms as described above with extrapolations from photospheric magnetograms. Results from this project are quite relevant to NASA's SOHO mission since the EUV emission line diagnostic techniques evaluated and implemented in this analysis comprise test case studies of SOHO (particularly CDS) capabilites. Furthermore, the active region and quiet-sun averaged spectra derived in this work have been provided to and used by the TRACE and Solar-B teams in preparation for those missions.

The observations were obtained with NASA/GSFC's Solar EUV Rocket Telescope and Spectrograph (SERTS), the Very Large Array (VLA), and magnetographs. When the proposal requesting NASA support for this project was submitted back in September of 1993, the quality of the data from the SERTS flight of 17 August 1993 was not yet known. The proposal stated, however, that if those data became available and were of sufficiently high quality, they would be analyzed in addition to the data from the 1991 flight. Since the data from the 1993 flight were found to be of excellent quality, I analyzed data from both flights simultaneously.

2 Results

SERTS spectral data from both the 7 May 1991 and the 17 August 1993 flights were analyzed simultaneously. For each flight, digitized, calibrated spectral arrays and spectroheliograms were provided by Drs. Joseph Davila and Roger Thomas of the Laboratory for Astronomy and Solar Physics at NASA/GSFC. Since the 1993 data were cleaner and less noisy that the 1991 data, I concentrated more on the 1993 data for purposes of coronal magnetography. VLA 20 and 6 cm microwave images for both dates were provided by Drs. Stephen White and N. Gopalswamy of the University of Maryland Solar Radio Group.

2.1 Spatially Averaged Spectra

For the 1993 and 1991 flights I sought and removed plate flaws from the digitized SERTS spectral data (20,000 x 80 arrays). I then selected appropriate portions of the slit and obtained averaged spectra for quiet-sun areas, AR 7563, AR 6615, and areas above the limb. After correcting the spectra for background, I fitted emission line candidates with Gaussian profiles and compiled lists of reliably detected lines. Using line intensities from the averaged specta, I then compared the measured and theoretical values for numerous density- and temperature-insensitive line intensity ratios. A systematic discrepancy between the measured and theoretical values in all of the averaged spectra indicated an unexpected inconsistency in the SERTS photometric calibration. This was and still is extremely puzzling, since the laboratory calibration measurements were clean and reproducible. This problem was circumvented by revising the photometric calibration such that the measured density- and temperature-insensitive line intensity ratios agreed with their corresponding theoretical values. All subsequent analyses were based upon this revised calibration. Table 1 lists the theoretical and the measured values for numerous density- and temperature-insensitive line intensity ratios.

The problem with and the correction of the SERTS instrumental calibration underscore the value of accurate atomic physics calculations. The bottom line is that spectrographs like SERTS can be calibrated with accurately known emission line ratios. Furthermore, the ability to use emission line ratios to calibrate a spectrograph indicates the self-consistency and overall validity of relevant atomic physics parameters for numerous ions obtained from a variety of sources. Knowing this, one can confidently extract plasma parameters from the SERTS spectra as well as from SOHO/CDS spectra.

2.2 Density and Temperature

Densities were derived from density-sensitive line intensity ratios within a given ion species, and temperatures were derived from ratios of line intensities in two different ion species. As is evident from the values listed in Table 2, active region densities typically exceed quiet Sun densities, but not necessarily by large amounts. Note that the Fe XII ion consistently yields high densities. Note also that numerous ratios are available for the Fe XIII ion. For all of the listed ratios of this ion, the 1993 active region, 1991 active region, and 1993 quiet sun yield density logarithms of 9.66 ± 0.49, 9.60 ± 0.54, and 9.03 ± 0.28, respectively. For comparison, Dere *et al.* (1979, ApJS, 40, 341) found order-of-magnitude (lower to upper limit) uncertainties on solar flare densities derived from individual line ratio measurements from Skylab data.

Filling factors were derived by combining measurements of the line intensities, calculations of the plasma densities, and the theoretical emissivities. Assuming a path length of $\Delta\ell = 1 \times 10^9$ cm, the derived filling factors range from much less than one to near unity.

Table 3 lists the temperatures derived from numerous temperature-sensitive line intensity ratios, *in the isothermal* approximation. The active regions are clearly hotter than the quiet sun for about half of the ratios listed in the table. However, for ratios which involve lines from only Fe XIII, XII, XI, and X, the active region and quiet sun temperatures are equal to within the derived

uncertainties.

Because SERTS spectra are spatially resolvable, one can discern spectral variations with position along the slit. The spectrum within each spatial resolution element is noisier than the spatially averaged spectrum, but numerous emission lines are identifiable. For each spatial resolution element, I obtained the spectral background, subtracted it from the original spectrum, and obtained the integrated line intensities for 20 key emission lines from the background-corrected spectrum. The procedure is similar to that used for the spatially averaged spectra. In this way, densities and temperatures can be derived as functions of position along the slit. Results are shown in Figures 1 and 2. Note that the temperature increase toward the active region core is small but statistically significant. Note too that the density remains constant across the slit (based on the measurement uncertainties), despite the fact that the emission line intensities vary substantially. This indicates that the product of the path length and the volume filling factor, $f\Delta\ell$, is greater in the active region core than it is in the outskirts.

2.3 Differential Emission Measure

Since each solar feature observed by SERTS manifests variety in its plasma density and temperature, it is useful to know the temperature distribution of the emitting material within each feature. Such information is obtained from a differential emission measure (DEM) analysis. We used the numerical procedure developed by Monsignori-Fossi and Landini in order to evaluate the active region and quiet-sun DEM in this work. These are shown in Figures 3 and 4. The active region DEM was extremely valuable in the subsequent calculation of coronal magnetograms.

2.4 Mass Flows

I examined the wavelength shifts along the slit for several bright lines formed in a variety of temperature regimes, and found no evidence for Doppler shifts due to mass motions in AR 7563. Lower limits on reliable detections for the strong lines of He II λ304 and Fe XVI λ335 are $\sim$ 10 km/sec. These are shown in Figure 5.

2.5 Coronal Magnetography

I used the differential emission measure derived from the spatially averaged active region spectrum in order to estimate the DEM in each spatial pixel of the two dimensional images. I was then able to calculate the thermal bremsstrahlung optical depth as a function of temperature in each pixel. It should be pointed out that use of the DEM is a different but better approach than the one originally planned. Briefly, I obtained a DEM for each spatial pixel in the two dimensional images by scaling the spatially averaged DEM based upon corresponding pixel intensities in the images of Mg IX λ368, Fe XV λ284, and Fe XVI λ335. The resulting DEM curves were integrated over small temperature intervals in order to obtain the column emission measure in those temperature intervals. The latter is a critical quantity for deriving the thermal bremsstrahlung optical depth. I also derived the temperature dependence of the density from the densities derived with the spatially

averaged spectrum. For each spatial pixel, the coronal magnetic field (as a function of temperature, B(T), since no absolute height scale was available) was allowed to vary. The solution for each pixel was the B(T) which minimized the differences between the observed and the calculated 20 and 6 cm intensities in that individual pixel. See Figure 6, which shows a comparison of observed and calculated 20 cm intensity contours overlaid on the VLA 20 cm intensity map. Note how closely matched the contours are (0.25, 0.50, 1.0, and 1.5 $\times 10^6$ K).

I found no evidence for cool, absorbing plasma in the solar corona above region 7563. I found that the free-free emission mechanism alone was not sufficient to produce the observed microwave brightness temperatures: gyroemission was also required. I successfully obtained a three dimensional coronal magnetic field which yields the observed brightness temperature distribution at two microwave observing frequencies (1.465 and 5.0 GHz). Figure 7 shows a two dimensional coronal magnetogram at log T = 6.0 (contours are 100, 150, 175, 200, and 250 Gauss); similar maps are available over a wide range in temperature values. Although the uniqueness of the solution cannot be firmly established (in light of the measurement uncertainties), the method is quite powerful and should be repeated with other similar data sets. The extrapolated coronal (heights $\sim$ 5,000 - 10,000 km) potential fields are inadequate to produce the observed microwave emission: the extrapolated fields are factors $\sim$ 2 too weak. Improvements could be made if more extensive density diagnostics were available, so that the temperature dependence of the density could be derived (rather than extrapolated) over a wider range of temperature. This would also provide more or better information on the volume filling factor, so that an adequate height scale may be derived.

3 Papers and Presentations

Following is a list of refereed publications that have resulted from this project:

(1) "Measuring Active and Quiet Sun Coronal Plasma Properties with EUV Spectra from SERTS," J. W. Brosius, J. M. Davila, R. J. Thomas, and B. C. Monsignori-Fossi, ApJS, vol. 106, in press, 1996.

(2) "The Structure and Properties of Solar Active Regions and Quiet-Sun Areas Observed in Soft X-Rays with Yohkoh/SXT, and in the Extreme Ultraviolet with SERTS," J. W. Brosius, J. M. Davila, R. J. Thomas, J. L. R. Saba, H. Hara, and B. C. Monsignori-Fossi, ApJ, submitted, 1996.

(3) "Coronal Magnetography of a Solar Active Region Using Coordinated SERTS and VLA Observations," J. W. Brosius, J. M. Davila, R. J. Thomas, S. M. White, and N. Gopalswamy, ApJ, submitted, 1996.

(4) "Evidence for Velocity Redistribution of He II Ions as a Means of Enhancing the 304 Å Emission Intensity," S. D. Jordan, J. W. Brosius, *et al.*, in preparation.

Following is a list of scientific presentations that have been given during the course of this project:

(1) "Measurements of Active and Quiet Sun Coronal Plasma Properties with SERTS EUV Spectra,"

J. W. Brosius, J. M. Davila, R. J. Thomas, B. C. Monsignori-Fossi, and J. L. R. Saba, presented at IAU Colloquium # 153 ("Magnetodynamic Phenomena in the Solar Atmosphere – Prototypes of Stellar Magnetic Activity"), held in Makuhari near Tokyo, Japan, May 22 - 26, 1995 (conference proceedings).

(2) "Solar EUV Spectroscopy with SERTS: Measurements of Active and Quiet Sun Properties," J. W. Brosius, J. M. Davila, R. J. Thomas, S. D. Jordan, and B. C. Monsignori-Fossi, presented at the "Eleventh International Colloquium on UV and X-Ray Spectroscopy of Astrophysical and Laboratory Plasmas," held in Nagoya, Japan, May 29 - June 2, 1995 (INVITED) (conference proceedings).

(3) "Measurements of Active and Quiet Sun Coronal Plasma Properties with SERTS EUV Spectra," J. W. Brosius, J. M. Davila, R. J. Thomas, and B. C. Monsignori-Fossi, BAAS, vol. 27, p. 962 (1995).

(4) "The Structure and Properties of Solar Active Regions and Quiet Sun Areas Observed With SERTS and Yohkoh", J. W. Brosius, J. M. Davila, R. J. Thomas, and H. Hara, Eos (Supplement), vol. 77, p. s218 (1996), and BAAS, vol. 28, p. 880 (1996).

TABLE 1: Density- and Temperature-Insensitive Line Intensity Ratios

Line Ratio	Theoretical	1993 AR	1993 QS	1991 AR	1991 QS	1991 L	1989 AR
Fe XVI 360.8/335.4	0.479	0.499±0.081	0.474±0.077	0.503±0.080	0.438±0.077	0.442±0.071	0.415±0.094
Fe XV 312.6/327.0	0.581	0.793±0.200	—	1.034±0.239	—	—	0.757±0.194
Fe XV 327.0/417.3	0.341±0.094	0.217±0.038	0.395±0.104	0.324±0.058	—	0.119±0.044	0.258±0.047
Fe XV 417.3/284.1	0.0307±0.0041	0.0417±0.0069	0.0260±0.0050	0.0276±0.0046	—	0.0534±0.0124	0.0448±0.0071
Fe XV 327.0/284.1	0.0095±0.0014	0.0090±0.0015	0.0103±0.0025	0.0089±0.0015	—	0.0063±0.0021	0.0116±0.0021
Fe XV 312.6/284.1	0.0055±0.0008	0.0072±0.0018	—	0.0092±0.0020	—	—	0.0088±0.0021
Fe XV 312.6/417.3	0.183±0.040	0.172±0.043	—	0.335±0.076	—	—	0.195±0.047
Fe XIV 274.2/334.2	1.62±0.40	1.77±0.33	1.48±0.37	2.95±0.57	2.55±0.93	1.99±0.38	1.60±0.26
Fe XIII 359.8/348.2	0.259	0.199±0.036	0.215±0.059	—	0.162±0.063	0.103±0.045	0.175±0.040
Fe XIII 320.8/311.6	6.94	—	4.00±0.75	—	3.81±1.53	3.70±1.48	4.22±1.25
Fe XIII 321.5/312.2	0.475	0.296±0.070	0.485±0.116	—	—	0.510±0.148	0.383±0.102
Fe XIII 320.8/359.7	1.31±0.25	1.00±0.16	0.86±0.15	1.46±0.31	0.90±0.26	0.91±0.18	1.17±0.20
Fe XIII 312.9/359.7	0.374±0.015	0.216±0.059	0.258±0.133	—	—	0.485±0.143	0.324±0.100
Fe XIII 311.6/359.7	0.189±0.035	—	0.216±0.042	—	0.236±0.101	0.245±0.101	0.278±0.081
Fe XII 346.9/364.5	0.343±0.028	0.447±0.075	0.370±0.061	0.587±0.116	0.555±0.120	0.580±0.103	0.287±0.049
Fe XII 352.1/364.5	0.683±0.017	0.739±0.121	0.758±0.124	0.899±0.172	0.965±0.182	0.859±0.144	0.618±0.100
Fe XII 346.9/352.1	0.502±0.030	0.605±0.102	0.488±0.080	0.653±0.125	0.575±0.124	0.675±0.119	0.465±0.081
Fe XI 369.2/352.7	0.303	0.339±0.084	0.274±0.068	0.624±0.177	0.388±0.123	0.239±0.112	0.292±0.053
Fe XI 341.1/369.2	0.969±0.160	1.185±0.303	1.015±0.256	0.873±0.255	1.358±0.450	1.757±0.838	0.984±0.202
Fe XI 341.1/358.7	1.58	1.18±0.27	1.25±0.28	1.02±0.30	4.08±2.35	—	0.514±0.103
Fe X 365.6/345.7	0.420	—	0.329±0.076	—	—	—	0.567±0.107
Mg VIII 311.8/315.0	0.199	0.170±0.039	0.298±0.077	—	—	—	0.313±0.068
Mg VIII 313.7/315.0	0.385±0.009	0.292±0.057	0.287±0.059	0.292±0.079	0.436±0.092	0.820±0.192	0.317±0.062
Mg VIII 317.0/315.0	0.228±0.005	0.241±0.052	0.289±0.055	0.327±0.077	0.175±0.053	0.398±0.123	0.227±0.059
Mg VIII 339.0/315.0	0.266±0.003	0.277±0.049	0.157±0.033	0.194±0.046	0.154±0.046	—	0.213±0.042
Ni XVIII 320.6/292.0	0.46	0.379±0.103	—	0.419±0.072	—	—	0.426±0.075
Si VIII 314.4/319.8	0.352±0.010	0.378±0.083	0.509±0.091	—	0.307±0.102	0.510±0.127	0.479±0.109
Si VIII 319.8/316.2	1.50±0.02	1.32±0.26	1.38±0.26	0.76±0.20	1.59±0.32	1.29±0.30	1.27±0.24
Si IX 342.0/349.9	0.337±0.063	0.225±0.041	0.301±0.062	0.296±0.101	0.357±0.073	0.507±0.109	0.210±0.043
Si IX 349.9/345.1	1.40±0.23	1.59±0.27	1.55±0.27	1.60±0.36	1.50±0.30	1.45±0.29	1.97±0.36
Si IX 296.1/345.1	1.69±0.33	2.18±0.43	1.15±0.24	3.74±1.02	0.88±0.24	1.52±0.31	2.93±0.62
Si IX 292.8/345.1	1.10±0.07	0.572±0.204	0.987±0.293	—	—	—	0.996±0.269

TABLE 2

Density Logarithms Derived from Line Intensity Ratios

Line Ratio	1993 AR	1993 QS	1991 AR	1991 QS	1991 L	1989 AR
Fe XV 321.8/417.3	9.41 0.22	--	--	--	--	9.86 0.31
Fe XIV 353.9/334.2	9.58 0.14	9.35 0.11	9.87 0.19	9.22 0.13	9.43 0.13	9.58 0.14
Fe XII 338.3/352.1	10.30 0.12	9.96 0.11	10.42 0.15	10.24 0.14	10.19 0.13	10.36 0.14
Fe XI 308.5/369.2	9.34 0.43	9.37 0.31	--	--	9.72 0.58	<10.71
Fe XIII 320.8/348.2	9.17 0.09	8.75 0.13	9.23 0.10	8.44 0.12	8.52 0.11	9.44 0.09
Fe XIII 359.7/348.2	9.26 0.10	8.93 0.15	9.06 0.16	8.51 0.19	8.62 0.15	9.51 0.14
Fe XIII 359.7/359.8	9.44 0.13	9.04 0.22	--	8.82 0.37	9.25 0.35	<9.63
Fe XIII 311.6/348.2	--	9.14 0.11	--	8.80 0.30	8.91 0.30	10.17 0.65
Fe XIII 318.1/320.8	10.14 0.20	9.32 0.23	10.13 0.22	10.91 0.60	9.97 0.24	10.25 0.19
Fe XIII 318.1/321.5	10.07 0.20	9.16 0.10	--	--	9.34 0.15	10.11 0.23
Fe XIII 318.1/312.2	9.68 0.18	9.17 0.10	9.61 0.20	--	9.38 0.14	9.94 0.18
Fe XIII 318.1/348.2	9.36 0.09	9.01 0.03	9.42 0.10	9.15 0.07	9.04 0.03	9.73 0.14

TABLE 3

Temperature Logarithms from Line Intensity Ratios Among Various Iron Ionization Stages

Line Ratio	1993 AR	1993 QS	1991 AR	1991 QS	1991 L	1989 AR
XVII 350.5/XVI 335.4	6.61±0.05	—	6.72±0.04	—	6.82±0.06	6.53±0.03
XVII 350.5/XV 284.1	6.52±0.03	—	6.59±0.02	—	6.60±0.02	6.52±0.02
XVI 335.4/XV 284.1	6.41±0.02	6.32±0.02	6.44±0.02	6.32±0.02	6.39±0.02	6.51±0.03
XVI 335.4/XIV 334.2	6.32±0.01	6.26±0.01	6.37±0.02	6.27±0.01	6.29±0.01	6.37±0.02
XVI 335.4/XIII 348.2	6.32±0.02	6.25±0.02	6.36±0.02	6.24±0.02	6.27±0.02	6.37±0.02
XVI 335.4/XII 352.1	6.29±0.01	6.24±0.01	6.32±0.01	6.23±0.01	6.25±0.01	6.32±0.01
XV 284.1/XIV 334.2	6.24±0.02	6.21±0.02	6.31±0.03	6.22±0.02	6.20±0.02	6.27±0.02
XV 284.1/XIII 348.2	6.27±0.03	6.22±0.02	6.32±0.03	6.21±0.02	6.21±0.02	6.31±0.03
XV 284.1/XII 352.1	6.25±0.01	6.21±0.01	6.28±0.01	6.20±0.01	6.21±0.01	6.27±0.01
XIV 334.2/XIII 348.2	6.31±0.04	6.22±0.03	6.32±0.04	6.19±0.03	6.22±0.03	6.37±0.04
XIV 334.2/XII 352.1	6.25±0.01	6.21±0.01	6.26±0.01	6.19±0.01	6.22±0.01	6.27±0.01
XIII 348.2/XII 352.1	6.19±0.05	6.20±0.05	6.19±0.05	6.20±0.05	6.21±0.05	6.17±0.05
XIII 348.2/XI 341.1	6.15±0.03	6.17±0.03	6.15±0.03	6.13±0.03	6.15±0.03	6.16±0.03
XIII 348.2/X 345.7	6.11±0.02	6.11±0.02	6.11±0.02	6.11±0.02	6.12±0.02	6.10±0.02
XII 352.1/XI 341.1	6.10±0.02	6.13±0.02	6.11±0.03	6.06±0.03	6.10±0.02	6.15±0.03
XII 352.1/X 345.7	6.07±0.01	6.07±0.01	6.08±0.01	6.06±0.01	6.08±0.01	6.07±0.01
XI 341.1/X 345.7	6.03±0.02	6.01±0.02	6.04±0.03	6.06±0.03	6.06±0.02	6.00±0.02

Figure 1

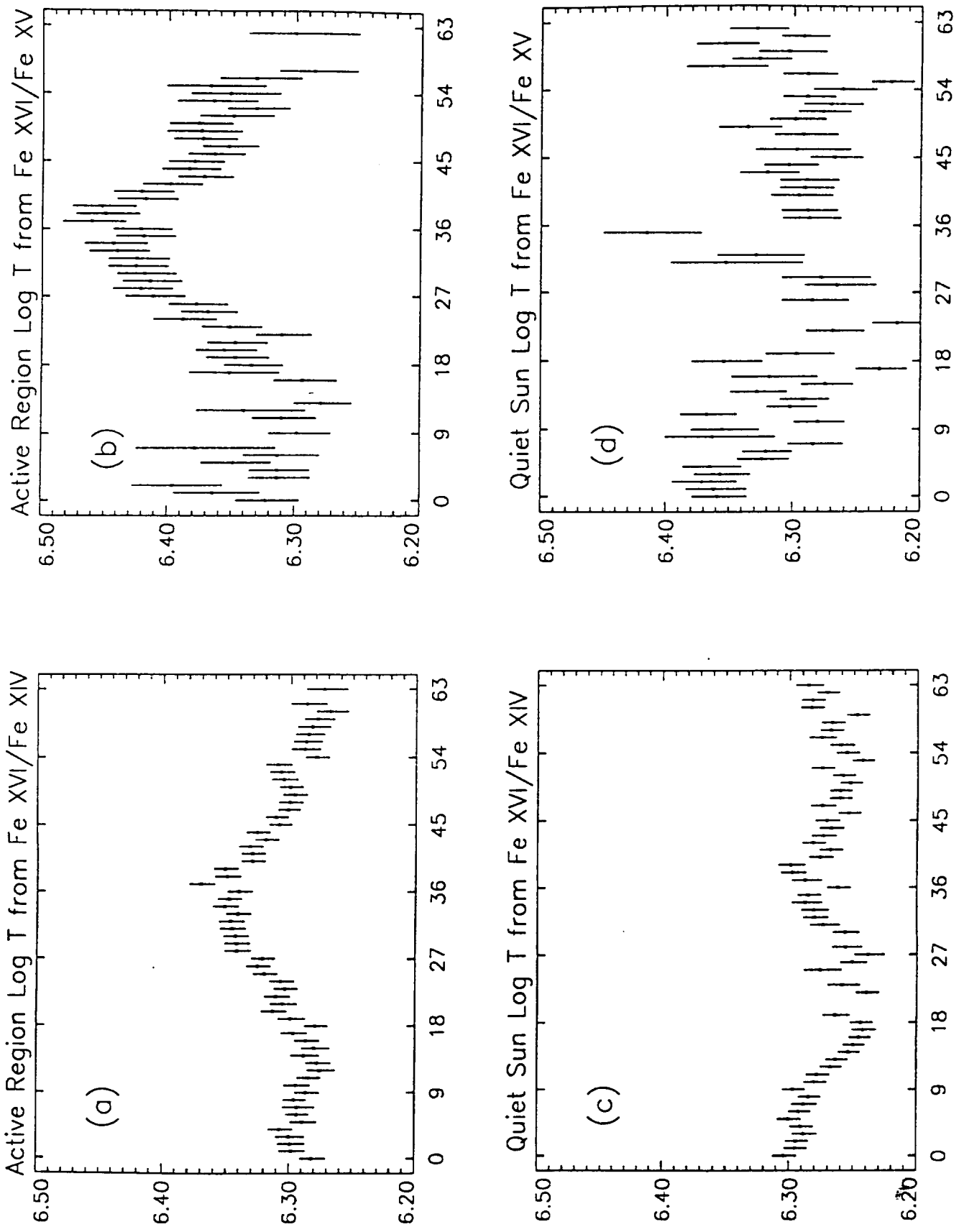
Active Region Log T from Fe XVI/Fe XIV
(a)
Active Region Log T from Fe XVI/Fe XV
(b)
Quiet Sun Log T from Fe XVI/Fe XIV
(c)
Quiet Sun Log T from Fe XVI/Fe XV
(d)
6.50
6.40
6.30
6.20
0
9
18
27
36
45
54
63

Figure 2

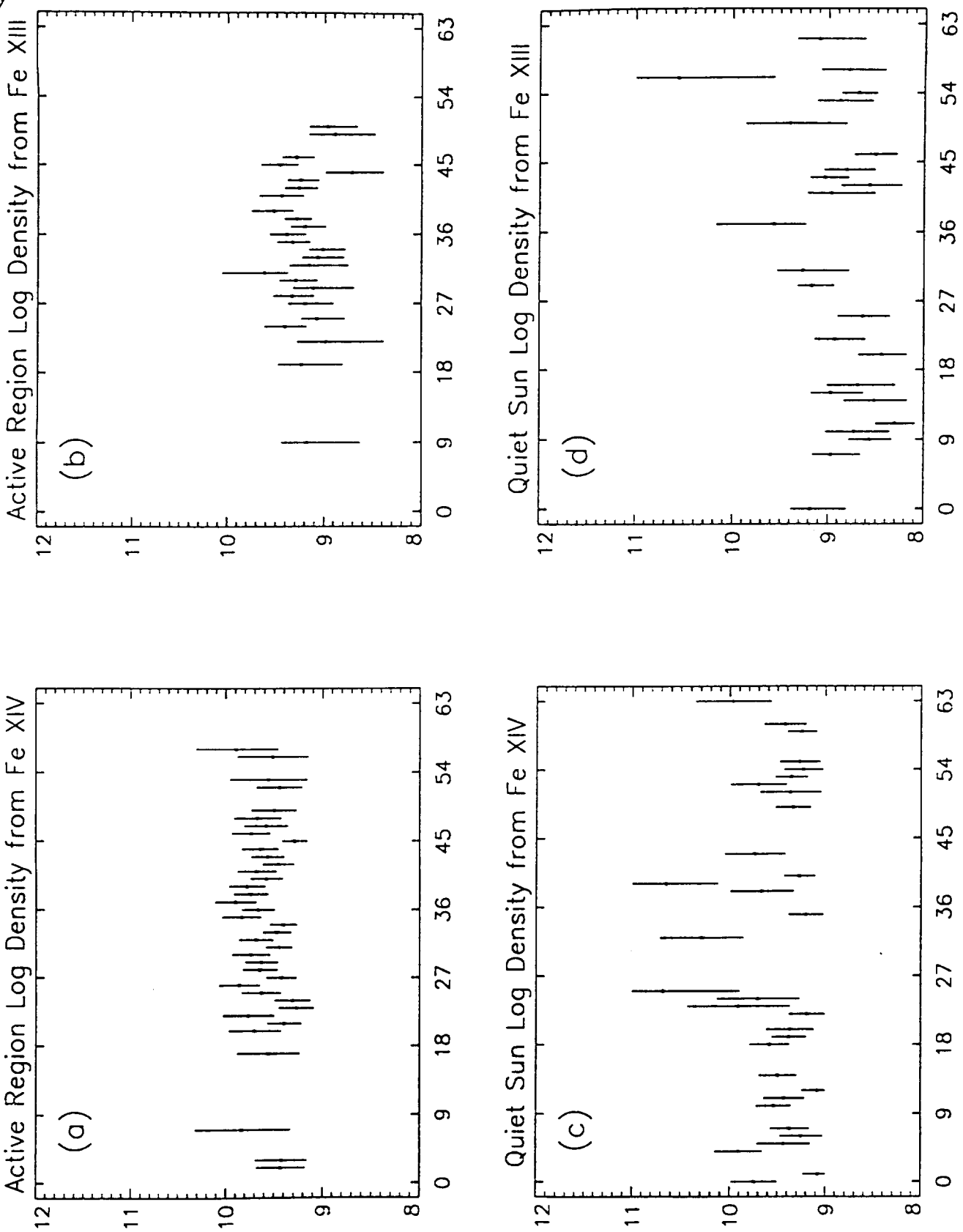
Active Region Log Density from Fe XIII
(b)
Quiet Sun Log Density from Fe XIII
(d)
Active Region Log Density from Fe XIV
(a)
Quiet Sun Log Density from Fe XIV
(c)
12
11
10
9
8
0
9
18
27
36
45
54
63

Fig. 3

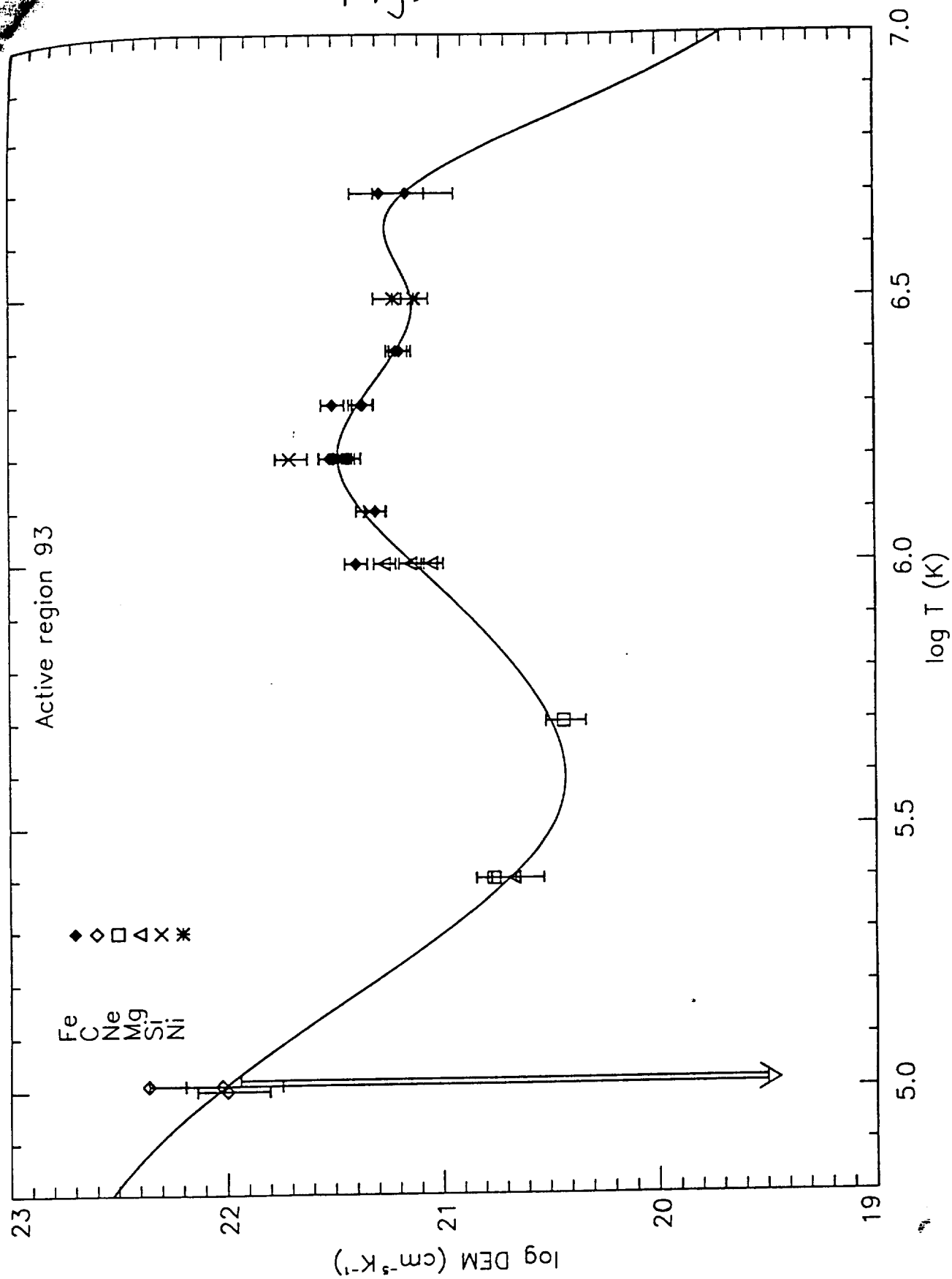
Active region 93
Fe
C
Ne
Mg
Si
Ni
log DEM (cm^{-5}K^{-1})
log T (K)
23
22
21
20
19
5.0
5.5
6.0
6.5
7.0

Fig. 4

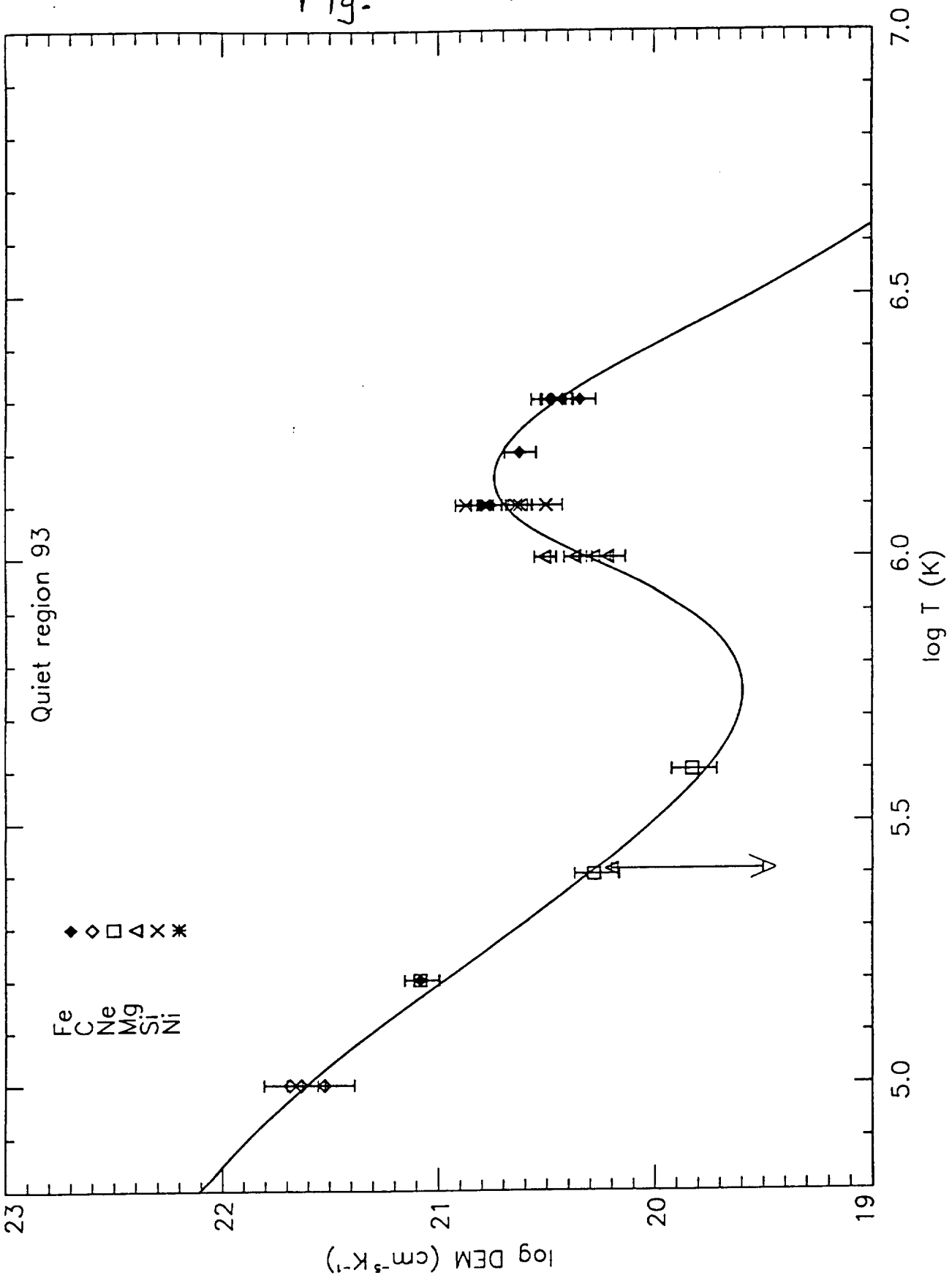
Quiet region 93
Fe
C
Ne
Mg
Si
Ni
log DEM (cm^{-5} K^{-1})
log T (K)
23
22
21
20
19
5.0
5.5
6.0
6.5
7.0

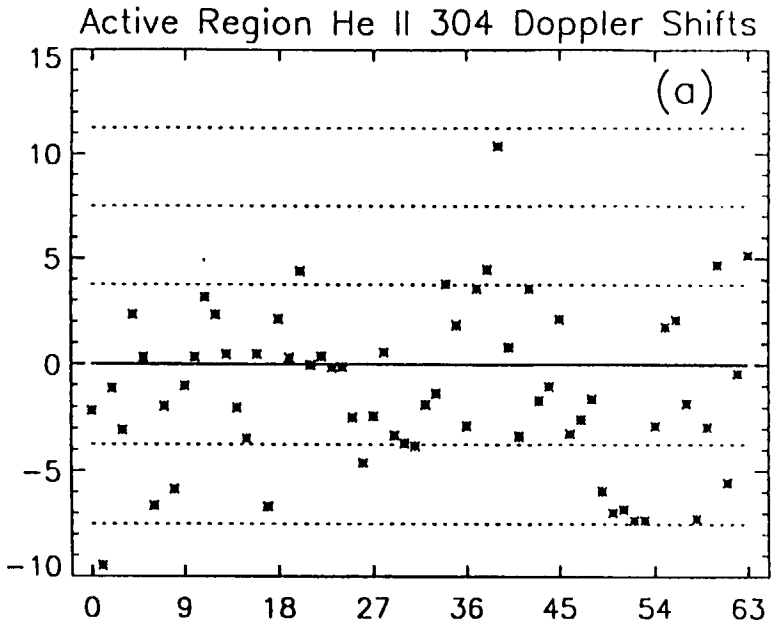
Active Region He II 304 Doppler Shifts
(a)
15
10
5
0
−5
−10
0
9
18
27
36
45
54
63

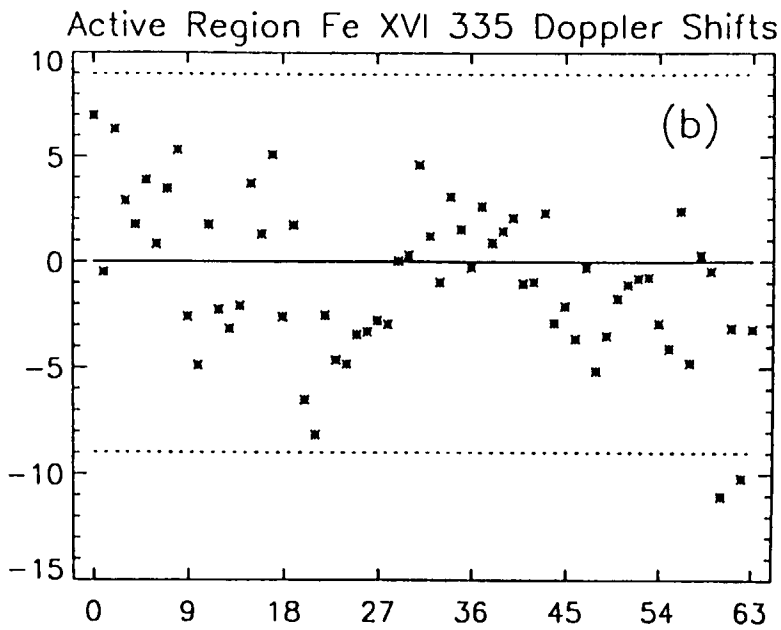
Active Region Fe XVI 335 Doppler Shifts
(b)
10
5
0
−5
−10
−15
0
9
18
27
36
45
54
63

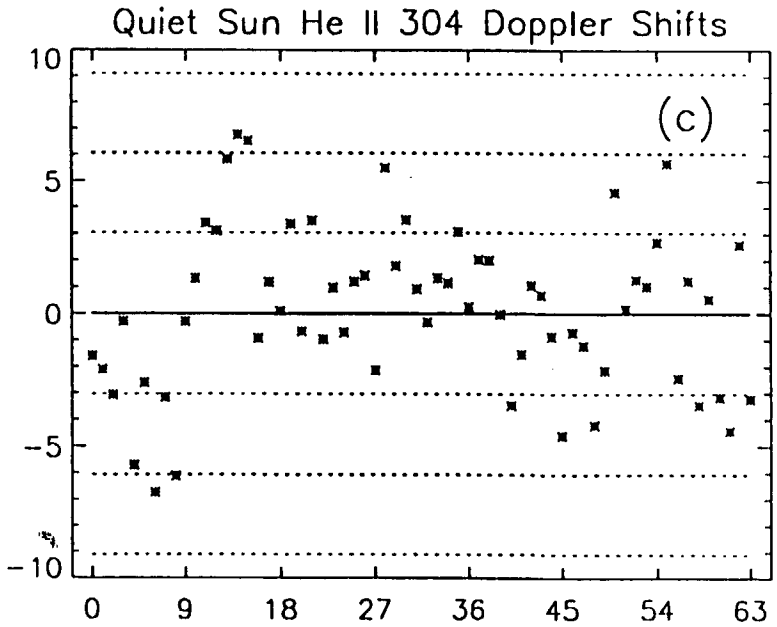
Quiet Sun He II 304 Doppler Shifts
(c)
10
5
0
−5
−10
0
9
18
27
36
45
54
63

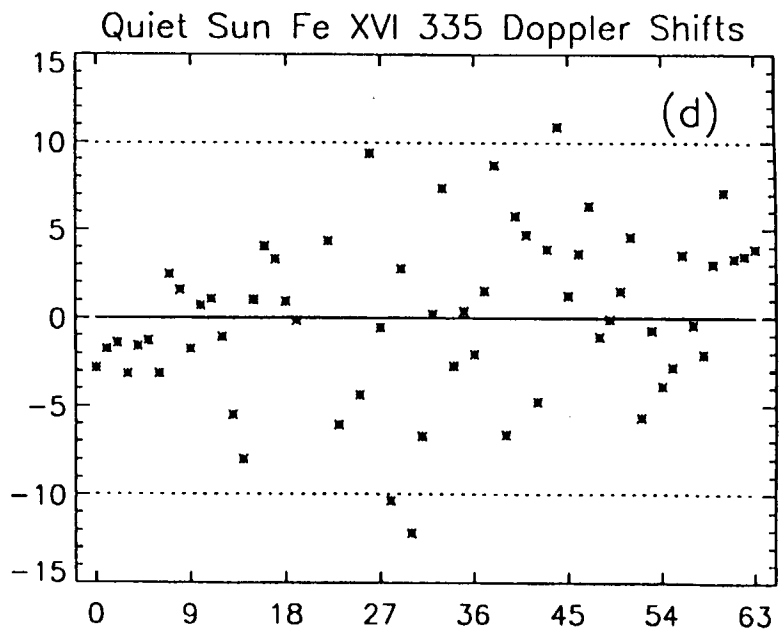
Quiet Sun Fe XVI 335 Doppler Shifts
(d)
15
10
5
0
−5
−10
−15
0
9
18
27
36
45
54
63

Figure 5

Fig. 6

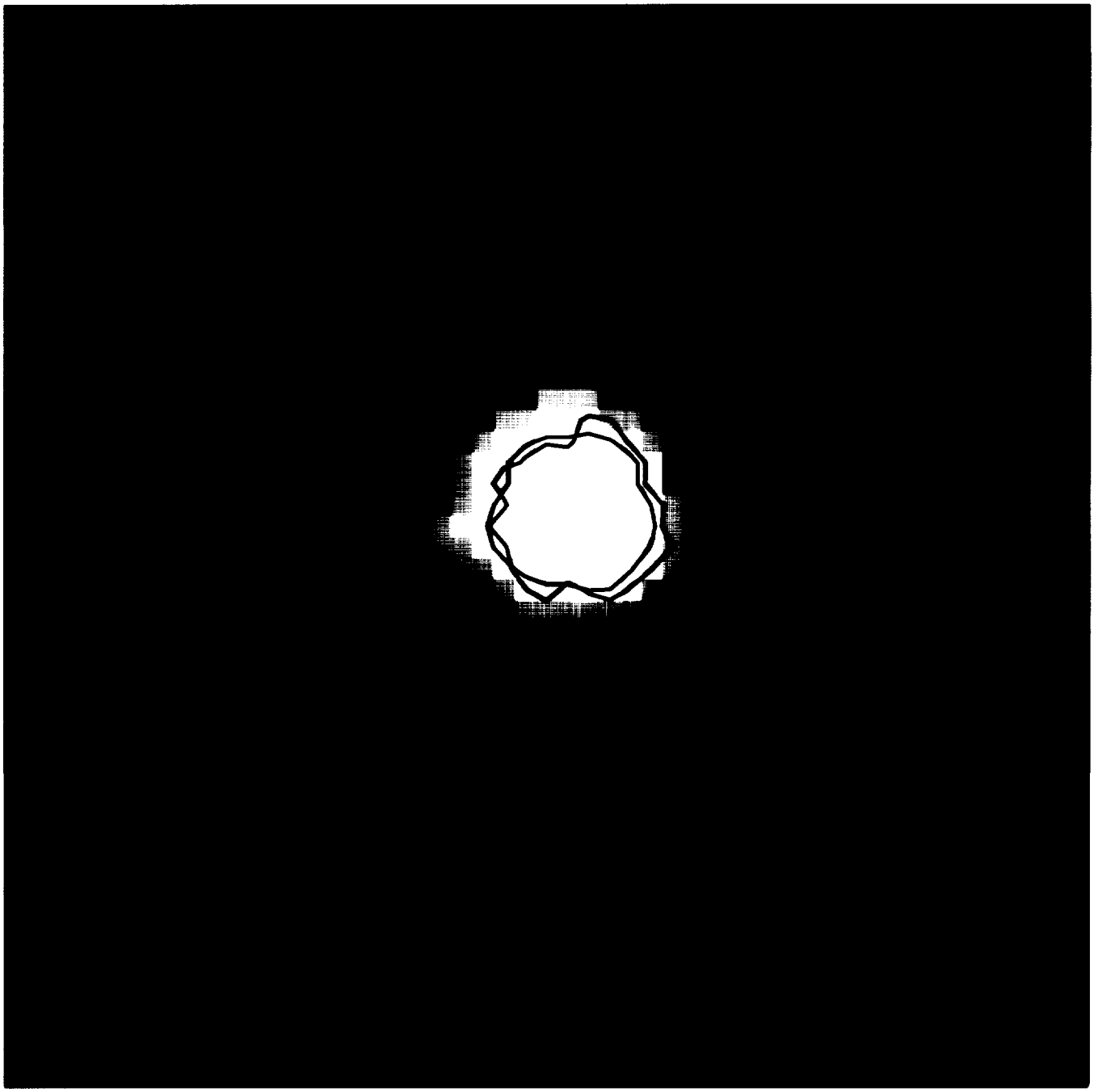

Fig. 7

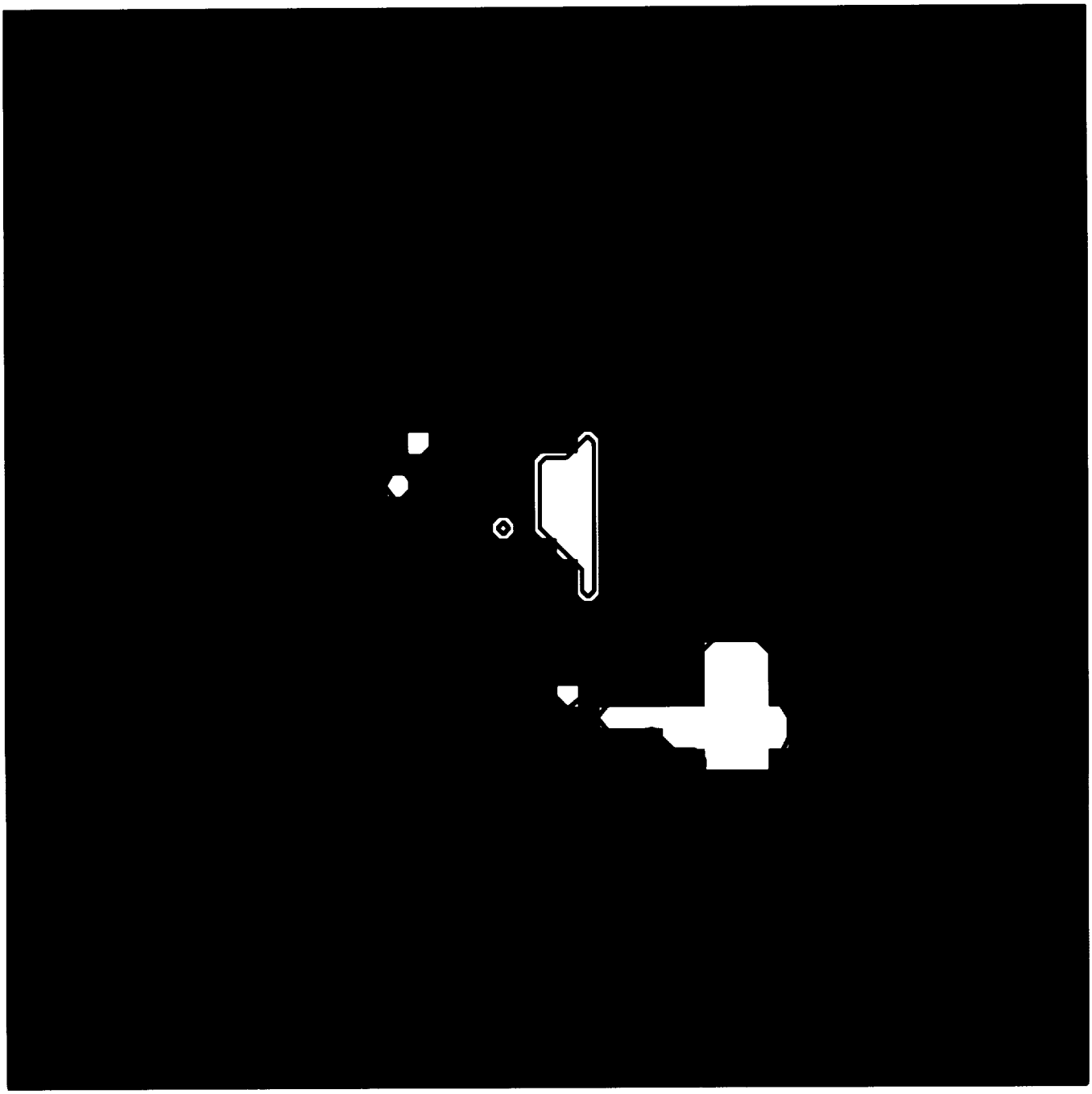

NASA REPORT DOCUMENTATION PAGE (IN LIEU OF NASA FORM SF 298)

1. REPORT NO.	2. GOVERNMENT ACCESSION NO. / 3. RECIPIENT'S CATALOG NO.
4. TITLE AND SUBTITLE Plasma Properties and Magnetic Field Structure of the Solar Corona, Based on Coordinated Max '91 Observations from SERTS, the VLA, and Magnetographs	5. REPORT DATE 26 July 1996 6. PERFORMING ORGANIZATION CODE:
7. AUTHOR(S) Dr. Jeffrey W. Brosius	8. PERFORMING ORGANIZATION REPORT NO:
9. PERFORMING ORGANIZATION NAME AND ADDRESS Hughes STX Corporation 4400 Forbes Blvd. Lanham, MD 20706	10. WORK UNIT NO. 11. CONTRACT OR GRANT NO. NASW-4933
12. SPONSORING AGENCY NAME AND ADDRESS Solar Physics Branch Space Physics Division Code SS NASA Headquarters Washington, DC 20546	13. TYPE OF REPORT AND PERIOD COVERED Final progress report for 12 July 1994 - 11 July 1996 14. SPONSORING AGENCY CODE NASA HQ/ CODE SS
15. SUPPLEMENTARY NOTES	

16. ABSTRACT

I determined the plasma properties and magnetic field structure of the solar corona using coordinated observations obtained with NASA/GSFC's Solar EUV Rocket Telescope and Spectrograph (SERTS), the Very Large Array (VLA), and Kitt Peak photospheric longitudinal magnetograms. A problem was identified with the SERTS calibration as determined from laboratory measurements. A revised calibration curve was derived by requiring that the numerous available measured line intensity ratios agreed with their respective theoretical values. Densities were derived from line intensity ratios, and active region densities were found to typically exceed quiet sun densities by factors of only about 2. The active region density was found to remain constant across the SERTS slit, despite the fact that the emission line intensities vary significantly. This indicates that the product of the path length and the volume filling factor must vary significantly from the active region outskirts to the central core. Filling factors were derived and found to range from much less than one to nearly unity. I examined wavelength shifts along the SERTS slit in the spatially resolved spectra, but found no evidence for significant Doppler shifts in active region 7563 or in the quiet sun. The numerical procedure developed by Monsignori-Fossi and Landini was used to derive the active region and quiet sun differential emission measure (DEM) from the spatially averaged spectra. A DEM was estimated for each spatial pixel in the two dimensional active region images by scaling the averaged active region DEM based upon corresponding pixel intensities of SERTS Mg IX, Fe XV, and Fe XVI images. These results, along with density measurements, were used in an IDL computer code which calculated the temperature dependence of the coronal magnetic field in each spatial pixel by minimizing the difference between the observed and calculated 20 and 6 cm microwave brightness temperatures. Results have been summarized in 3 ApJ papers.

17. KEY WORDS (SUGGESTED BY AUTHOR(S)) EUV Spectra, Corona, Microwaves, Magnetic Fields	18. DISTRIBUTION STATEMENT Space Science, Solar Physics

19. SECURITY CLASSIF.	20. SECURITY CLASSIF.	21. NO OF PAGES	22. PRICE
None	None		